Resistance and friction stir spot welding of DP600: a comparative study

M. I. Khan*[1], M. L. Kuntz[1], P. Su[2], A. Gerlich[2], T. North[2] and Y. Zhou[1]

Efforts to reduce vehicle weight and improve crash performance have resulted in increased application of advanced high strength steels (AHSS) and a recent focus on the weldability of these alloys. Resistance spot welding (RSW) is the primary sheet metal welding process in the manufacture of automotive assemblies. Friction stir spot welding (FSSW) was invented as a novel method to spot welding sheet metal and has proven to be a potential candidate for spot welding AHSS. A comparative study of RSW and FSSW on spot welding AHSS has been completed. The objective of this work is to compare the microstructure and mechanical properties of Zn coated DP600 AHSS (1·2 mm thick) spot welds conducted using both processes. This was accomplished by examining the metallurgical cross-sections and local hardnesses of various spot weld regions. High speed data acquisition was also used to monitor process parameters and attain energy outputs for each process. Results show a correlation found among microstructure, failure loads, energy requirements and bonded area for both spot welding processes.

Keywords: Resistance spot welding, Friction stir spot welding, Advance high strength steel, DP600, Microstructure, Mechanical properties

Introduction

Interest in the application of advance high strength steels (AHSS), particularly within the automotive architecture, has resulted in increasing demands for reliable spot welding methods. The mechanical and metallurgical changes in AHSS after the resistance spot welding (RSW) operations are well documented in the literature;[1–3] however, much work is left to be done. The feasibility of automotive joining of AHSS using friction stir spot welding (FSSW) has been recently considered,[4,5] but the performance of welded joints is still generally unknown. The increased use of AHSS grades in the automotive architecture has emphasised the need to examine how FSSW joining directly compares with RSW.

Advance high strength steels sheet has been introduced into auto body closures and suspension components resulting in a recent focus on the weldability of these alloys.[6] Resistance spot welding is the primary sheet metal welding process in the manufacture of automotive assemblies. The embedded infrastructure coupled with its superior surface finish makes RSW the economically and aesthetically desirable process. The microstructure of DP600 grade AHSS results in mechanical properties that are ideal for automotive applications with a high strength to weight ratio; however, microstructural changes during RSW dramatically affect mechanical properties by transforming the base metal (BM) microstructure. To date, the microstructures and failure mechanisms in resistance spot welded DP600 have not been examined in great detail. This is essential to the integration of dual phase sheet material in today's automobiles. For example, interfacial fracture, which is believed to have detrimental effects on the crashworthiness of vehicles, is a common occurrence when resistance spot welding dual phase steels.[7]

The friction stir welding process was developed by TWI, Abington, UK[8] in 1991 as a novel method for joining aluminium alloys. Since that time the welding process has been employed in aerospace, rail, automotive and marine industries for joining aluminium, titanium, magnesium, zinc and copper alloys, as well as steel and thermoplastics in thicknesses ranging from 1 to 50 mm. During FSSW the rotating tool penetrates the sheets being welded and is then retracted producing a stir zone region that comprises a fine dynamically recrystallised microstructure. Experimental results in aluminium and magnesium alloy sheets have shown that a combination of plastic deformation and viscous dissipation during spot welding produces very high power densities ($\sim 10^{10}$ W m^{-3}),[9,10] heating rates from 275 to 400 K s^{-1} depending on the rotational speed used[11] and peak temperatures, which approach the solidus temperature of the material being fabricated.[12,13]

The resistance and friction stir spot welding processes are leading candidates for spot welding AHSS. The objective of this work was to compare the microstructural features of welds produced using these two processes. Metallurgical cross-sections and local hardness of various spot weld regions were examined. Data

[1]Centre for Advanced Materials Joining, University of Waterloo, 200 University Ave. Waterloo, ON N2L 3G1, Canada
[2]Department of Materials Science and Engineering, University of Toronto, 184 College Street, Toronto, ON M5S 3E4, Canada

*Corresponding author, email Ibraheem@rogers.com

Published by Maney on behalf of the Institute
Received 8 June 2006; accepted 10 September 2006
DOI 10.1179/174329307X159801

acquisition (DAQ) systems were used to measure the energy input required to achieve desired failure loads for both processes. The fracture mechanisms in overlap tensile shear testing were studied and the relationship among peak failure load, energy input and bonded area was determined. The comparison of AHSS weld properties enables a benchmark for the evaluation of the weld performance of both the RSW and FSSW processes, which is important in weld process selection and welding procedure design.

Experimental procedure

The chemical properties of the material used in this study are summarised in Table 1.

Resistance spot welding

The RSW samples were produced using a pneumatically operated single phase RSW machine (CenterLine Ltd, 250 kVA) with constant current control and a frequency of 60 Hz. A truncated class 2 electrode with 6·0 mm face diameter was used as per AWS standards for 1·22 mm thick sheet.[14] Cooling water flowrate and hold time also followed AWS recommendation of 4 L min^{-1} and 5 cycles respectively. The RSW machine was fully equipped with a DAQ system capable of recording load, displacement ($\pm$0·01 mm), current and voltage simultaneously as a function of time. A linear transducer mounted to the top electrode measures the displacement while a calibrated coil collects the dI/dt, which is conditioned to attain current as a function of time. The load cell located under the bottom electrode measures the force applied by the overhead cylinder. The data acquisition rate was 25 000 points s^{-1} (pps). Figure 1 shows the typical DAQ output for a resistance spot weld.

Resistance spot welding samples were produced over a range of force, current and time parameters. A weldability test was conducted to determine weld lobes which produce acceptable weld quality as determined by AWS standards.[12] The weld current was varied from 7 to 9 kA, the weld force ranged from 3·5 to 5·5 kN, and the weld time was between 10 and 20 cycles. The weld parameters optimised for tensile shear strength and button size were 8 kA, 3·5 kN and 20 cycles. The weld samples were subjected to overlap tensile shear testing, coach peel testing and metallographic examination. A total of 11 tests were conducted per condition including five tensile tests, five peel tests and one sample for metallographic preparation.

The energy supplied Q_{RSW} during RSW is a product of the weld power and time, where the weld power is a product of the measured current I and voltage V. In this work, Q_{RSW} was calculated using equation (2) where $1 \leqslant n \leqslant N$ and Δt is the sampling time[15]

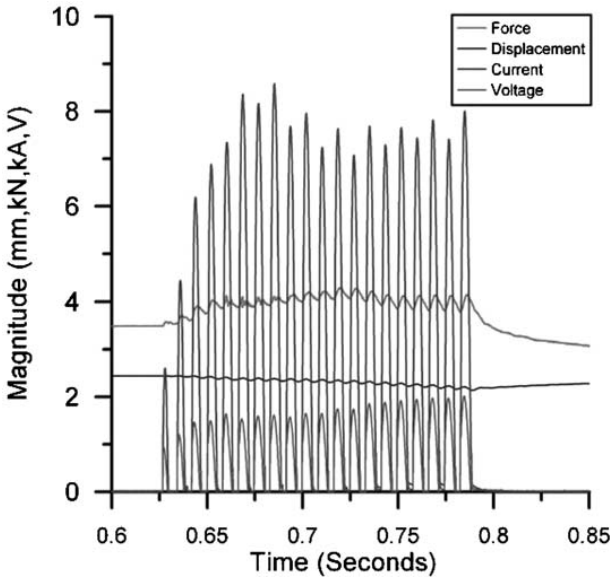

1 Data acquisition output for RSW

$$Q_{RSW} = \sum_{n=1}^{N} |I(n)| \cdot |V(n)| \Delta t \quad (1)$$

Friction stir spot welding

Friction stir spot welding welds were produced using a StirSpot welder (Friction Stir Link Inc.). Capabilities of this particular machine include tool rotational speed of up to 3000 rev min^{-1}, an axial load of 14 kN and plunge rates (tool displacement rate) from 0·1 to 25 mm s^{-1}. The W–25 wt-%Re tool used for the spot welds had a truncated cone geometry, a pin diameter of 4 to 5·1 mm, a pin length of 1·7 mm, and a shoulder diameter of 10 mm.

Samples were produced for mechanical testing used using a range of plunge rate and plunge depth settings. The plunge rates were 0·5 and 1 mm s^{-1} while the plunge depths varied from 1·7 to 2·1 mm. In all cases the tool penetration depth was measured using a linear transducer with an accuracy of $\pm$0·01 mm while the spindle revolution per minute was measured using a shaft encoder, which had an accuracy of $\pm$30 rev min^{-1}. The axial load and the torque values were measured using a six axis load cell, which was coupled with a DAQ system so that the axial force, torque and penetration depth values were recorded simultaneously during each spot welding operation. Figure 2 shows the typical output produced during FSSW of the DP600 sheet. For an explanation of the observed changes in axial force and torque during the FSSW operation the literature should be referenced.[12,16]

During linear friction stir welding, where the rotating tool is traversed across the joint, inert gas is required to

Table 1 Material properties of DP600

			Alloying elements, %				
Steel	Thickness, mm	Coating	C	Mn	Mo	Cr	Si
DP600	1·22	Hot dip galvanised	0·1	1·523	0·195	0·197	0·156

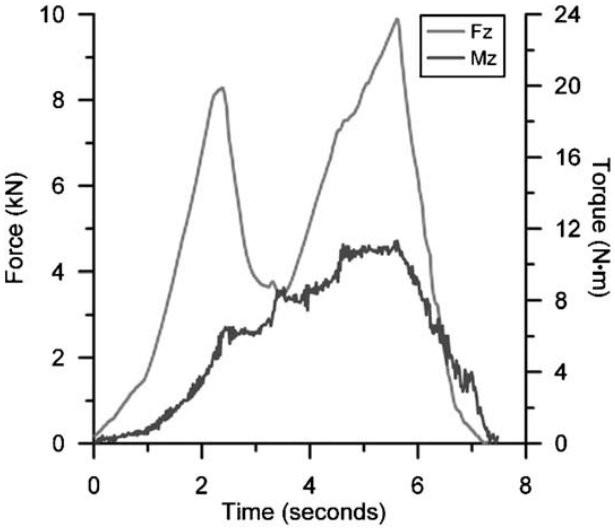

2 Data acquisition output for FSSW

shield the weld. Experimental results have shown that shielding gas is not required for spot welds where the tool is stationary (i.e. does not traverse parallel to the sheet). There was no difference between welds with and without Ar gas shielding, except for minor oxidation of the keyhole and upper surface of the weld occurring after tool retraction upon completion of the weld. After this, no gas shielding was used for the samples prepared for metallographic inspection and mechanical testing.

The energy applied during FSSW (Q_{FSSW}) is the sum of the normal and vertical components. Equation (2) was used along with the experimentally measured normal force F and displacement x; and, the axial torque T and angular velocity ω.[17] The sampling time was Δt and $1 \leqslant n \leqslant N$

$$Q_{\mathrm{FSW}} = \sum_{\mathrm{n}=1}^{\mathrm{N}} F(n)\cdot[x(n)-x(n-1)] + \sum_{\mathrm{n}=1}^{\mathrm{N}} T(n)\cdot\omega(n)\cdot\Delta t \quad (2)$$

During metallographic examination all test sections were etched using Lepera's reagent to distinguish the different phases in the fusion zone (FZ), heat affected zone (HAZ), stir zone and thermomechanically affected zone (TMAZ) for both RSW and FSSW processes.[18] When this particular etchant is used, martensite is etched white, α-ferrite is tan coloured and bainite is black.

Joint mechanical properties were evaluated by measuring the peak load to failure during overlap tensile shear testing. Table 2 shows specimen dimensions. Care was taken to maintain coplanar alignment during mechanical testing. The fracture surfaces of broken overlapped shear test specimens were examined using SEM fractography. Detailed examination of failure mechanism was also facilitated by interrupting the loading cycle during overlap shear testing, i.e, by halting the tensile testing machine when the welded section had only partially failed. This technique allowed detailed examination of the nature of failure propagation during failure of particular joints. Finally, the projected cross-sectional area of the bonded region was measured by digital image analysis.

Table 2 Specimen dimensions

Specimen	Length, mm	Width, mm
RSW	120	40
FSSW	100	25

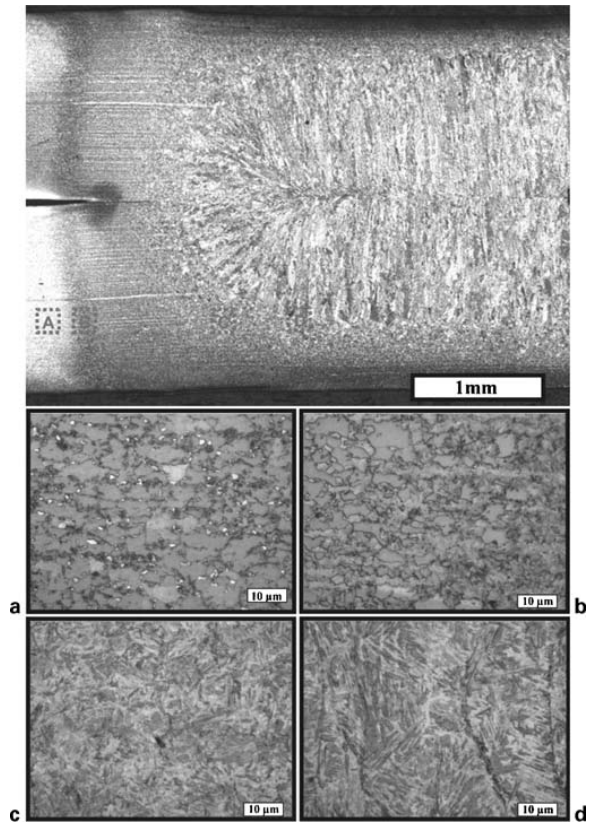

a base metal; *b* HAZ; *c* coarse grain region; *d* fusion zone

3 Microstructure for different weld sites in RSW

Microhardness testing of DP600 steel sheet was carried out using a Shimadzu HMV-2 Vickers microhardness testing machine with a 200 g load and a holding time of 10 s. Microhardness testing with 0·2 mm grid spacing revealed the hardness distribution and the individual hardness values in selected regions of welded joints. Different sample were used for RSW and FSSW welds in order to accommodate the sample fixtures used. Other work has shown that increasing the sample dimensions in FSSW has no effect on properties.

Results

Resistance spot welding

A representative RSW weld cross-section is shown in Fig. 3 (8 kA, 3·5 kN, 20 cycles). The FZ, HAZ and BM can be clearly observed. Microstructural observations of these regions are shown in Fig. 3*a–d*. A hardness profile of the weld region is shown in Fig. 4. This profile shows the hardness in the BM, HAZ and FZ regions.

The BM in Fig. 3*a* shows the typical finely dispersed martensite particles (white) surrounded by a ferrite matrix (fawn) that are characteristic of the automotive dual phase steels. Peak temperatures during welding in this region are typically below the martensite tempering temperature (i.e. $<200^{\circ}$C). Hardness values in the BM range from 150 to 200 HV, which is an indication of the mainly ferritic nature of the microstructure.

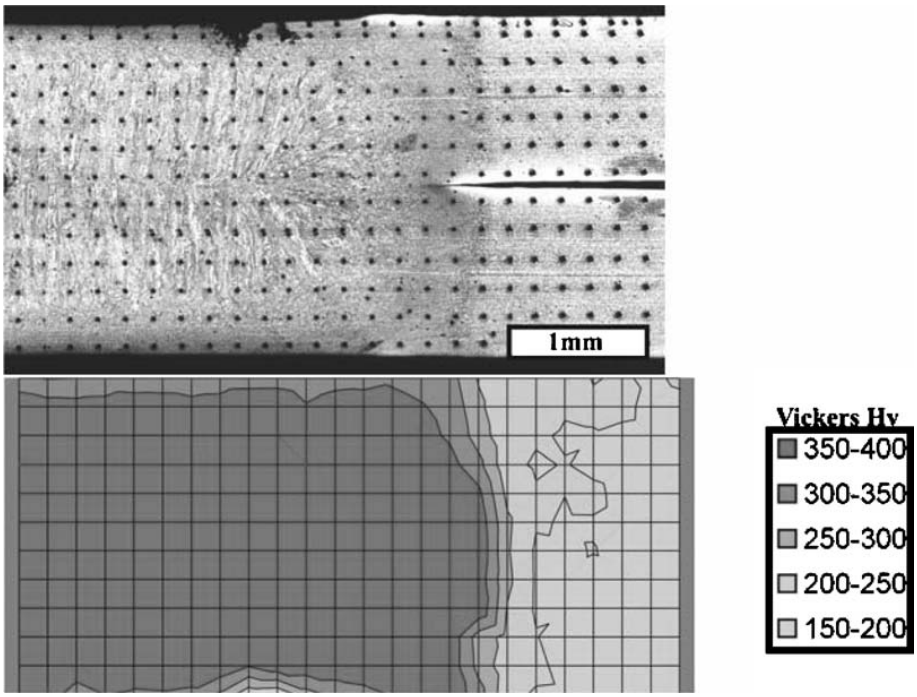

4 Microhardness maps of RSW cross-section

In the HAZ, the volume fraction of martensite increased. The peak temperature during welding in this region ranges from martensite tempering temperatures to just below the liquidus. Figure 3*b* shows a transitional region from the intercritical (IC) to the fine grained region (FG) within the HAZ. Peak temperatures in the IC region are between the Ac1 and Ac3, resulting in a coarsening of the martensite phase. Within the FG region, temperatures exceed the Ac3 resulting in complete austenitisation. The austenite is inhomogenous owing to the nature of segregation within the DP microstructure and short time above Ac3; resulting in the banding nature of martensite and the formation of fine grained ferrite. Hardness values in this area exceed that of the BM, 230–280 HV, which indicates an increase in the volume fraction of martensite with a ferrite matrix.

Within the HAZ, the peak temperature is well above Ac3, resulting in complete austenitisation and grain growth. The grain coarsened (GC) region consists of prior austenite grains about 10–15 μm in diameter. The microstructure in the GC region is blocky martensite, as shown in Fig. 3*c*, with a hardness in excess of 350 HV (Fig. 4).

The FZ shown in Fig. 3*d* is characterised by the columnar nature of solidification. The microstructure consists of large equiaxed columnar martensite grains. From Fig. 4 it can be seen that hardness values are similar to those in the HAZ region, ranging above 350 HV.

Friction stir spot welding

Figure 5 shows the microstructural features observed at different locations relative to the keyhole centreline in a FSSW spot weld in DP600 sheet. The BM was similar to the RSW case, with martensite islands in a ferrite matrix with a hardness up to 200 HV. The IC region of the HAZ, as shown in Fig. 3*b*, is significantly wider than the RSW case owing to the longer weld times. The hardness in this region was ~220 HV, as shown in Fig. 6.

Beyond the HAZ and towards the keyhole, in the TMAZ region the microstructure is comprised of a mixture of lath martensite and fine acicular ferrite, as shown in Fig. 5*c*. This region is subject to temperatures above Ac3 and high strain rates, resulting in dynamic recrystallisation and grain growth. The prior austenite grain size in this location was markedly increased. The

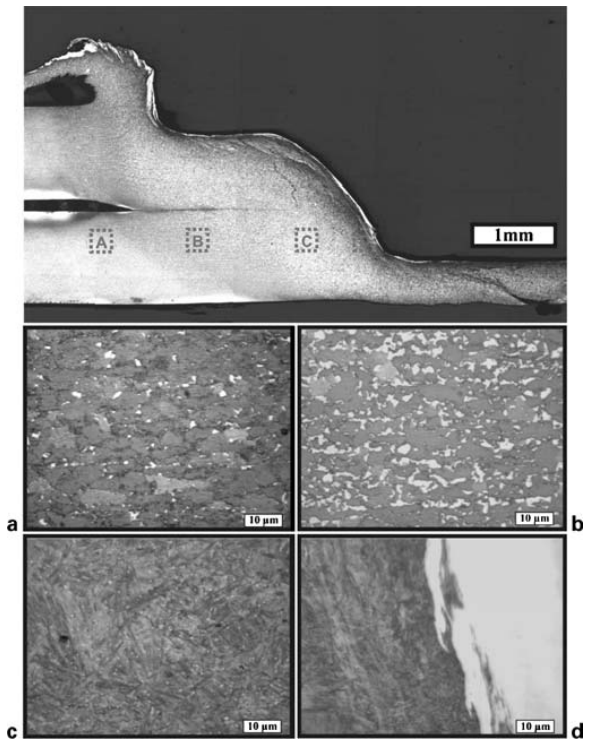

a base metal; *b* HAZ; *c* TMAZ; *d* stir zone

5 Microstructure for different weld sites in FSSW

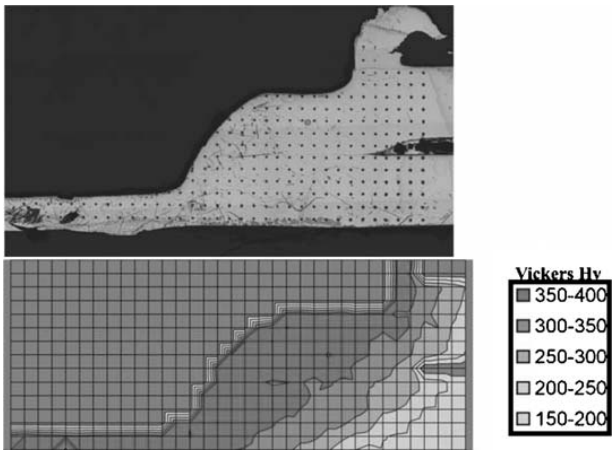

6 Microhardness maps of FSSW cross-section

hardness in the TMAZ was ~300 HV (Fig. 6). In addition to the lathy martensitic microstructure, fine particles or rods of martensite which are <1 μm in diameter are observed, which will be the subject of further communications.

Immediately beside the keyhole periphery the stir zone microstructure is comprised of very fine grain martentsite that could not be observed using optical microscopy (Fig. 5*d*). The grain size in the stir zone of friction stir spot welds are typically <10 μm in FSSW.[12] The hardness in this particular location was ~350 HV, as shown in Fig. 6.

The top surface of the FSSW welds shows a poor finish with a keyhole resulting from the pin, and an indentation surrounded by expulsion, or debris, caused by the tool shoulder. Discoloration of the surface is a result of oxidation; however, this may be prevented by Ar shielding if desired. Figure 7*b* shows a typical surface for FSSW. Compared with FSSW, the typical surface appearance for RSW is considered more acceptable for automotive applications. As shown in Fig. 7*a*, the surface is smooth with a slight indentation and discoloration of the galvanised coating resulting from the thermal effects of the welding process.

Tensile shear testing

Cross-sections of partial tensile shear test specimens can be used to observe failure propagation. Figure 8 shows a

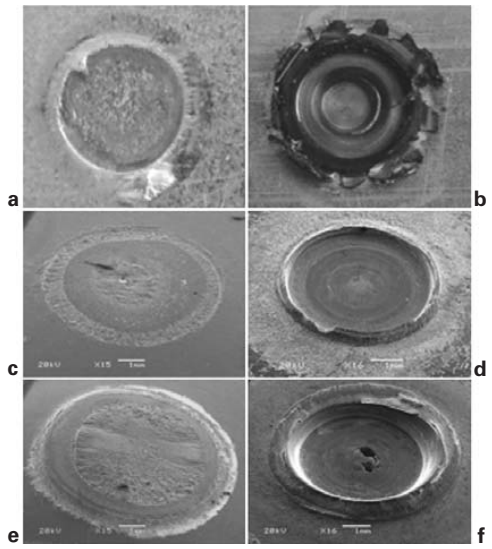

a **RSW weld surface;** ***b*** **FSSW weld surface;** ***c*** **low energy RSW input;** ***d*** **low energy FSSW input;** ***e*** **high energy RSW input;** ***f*** **high energy FSSW input**

7 Weld and fracture surface for RSW and FSSW

partially failed tensile shear test result for a RSW sample welded under the condition of 8 kA current, 3·5 kN force and 20 cycles weld time. The fracture extends from the faying surface interface at the fusion boundary into the FZ along the weld centreline. Figure 9 shows an FSSW cross-section along the side where crack initiation occurs for partial tensile test specimen. This weld was produced under optimal welding condition (3000 rev min^{-1}, 2·1 mm penetration, 0·5 mm s^{-1} plunge rate**)**. The fracture initiates from the tip of the unbonded interface, and propagates through the stir zone in the upper sheet.

Figure 7*c–f* shows the fracture surfaces produced in failed overlap shear testing specimens made using high and low energy input values. Low and high energy inputs produced an interfacial fracture through the FZ of the resistance spot weld (Fig. 7*c* and *e*). When a low energy input was applied during FSSW the welded joint failed across the weld zone at the interface of the two sheets**.** When high energy inputs were applied the mode of failure involved a partial pull-out (Fig. 7*f*). There was

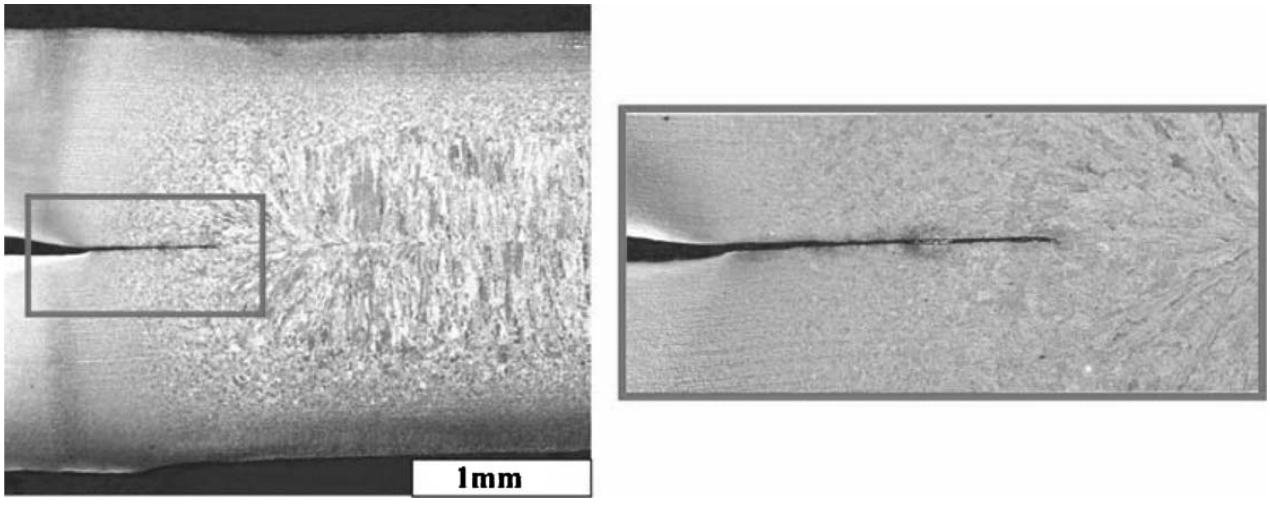

8 Partial tensile of RSW cross-section

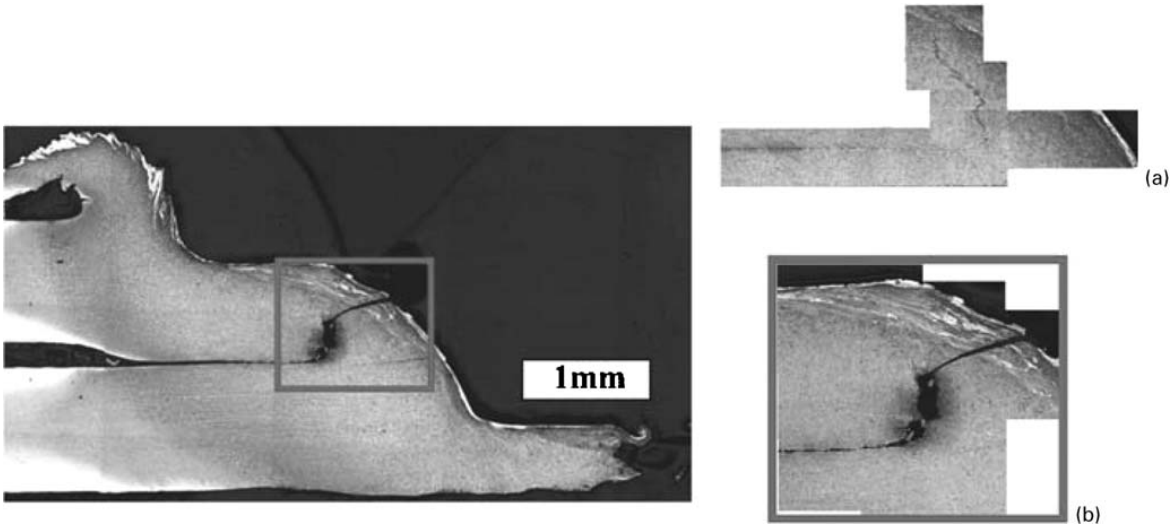

a as welded; *b* partial fracture

9 Partial tensile of FSSW cross-section

no change in failure mechanism observed with changes in heat input.

Discussion

Microstructure and hardness

The microstructure and hardness in the weld regions of both RSW and FSSW had similar microstructural features. The IC and FG regions of the HAZ consist of a mixture of martensite and ferrite. The hardness in these regions reaches up to 280 HV.

The FSSW weld contains unique regions that are not found in the RSW case. The RSW weld microstructure shows a CG region beside to the fusion boundary. The microstructure is predominately martensite as indicated by the high hardness values (350 HV). The FSSW weld microstructure contains a region termed the TMAZ beside the HAZ. This region consists of a mixture of hard martensite rods, lathy martensite, and bainite or acicular ferrite. The hardness in this region is 300 HV, slightly lower than the CG region in the HAZ owing to the microstructure mixture. In both the TMAZ of FSSW and CG regions of the RSW welds respectively, the prior austenite grain size is large.

The FZ in the RSW weld consists of a hard martensitic columnar microstructure in excess of 350 HV. This compares well with the fine grained FSSW stir zone microstructure hardness of 350 HV.

There is a gradual transition in hardness from the stir zone through the TMAZ and into the HAZ of the FSSW weld (Fig. 6). The hardness gradient is much steeper in the RSW weld as a result of the smaller HAZ size (Fig. 4). The heat input for the FSSW process is higher than the RSW process, resulting in a HAZ that is significantly larger than the RSW weld. The hardness gradient and size of the HAZ have no effect on weld tensile properties at low strain rates.

The keyhole produced by the stir tool decreases the bonded area for a given weld size. This necessitates a comparison of the weld size based on bonded area rather than weld diameter. The bonded area as a function of total weld energy is shown in Fig. 10. There is a clearly increasing trend in weld area with increasing weld energy. Furthermore, the ratio of weld area to total energy is similar for both the RSW and FSSW processes. This shows that the weld efficiency of both processes is similar.

Fracture analysis and mechanical properties

Taking into account the unbonded region located near the TMAZ, both FSSW and RSW welds are bonded with a zone consisting predominately of martensite, with hardness values >350 HV. Partial tensile results from Figs. 8 and 9 show the location of fracture initiation within the weld. From Fig. 8 the fracture for RSW welds initiates at the interface and continues through the coarse grain region towards the centreline structure. This sequence indicates fracture occurring through a brittle median. A similar brittle path is followed with FSSW welds where the crack initiates at the tip of the unbonded region and propagates through the stir zone under the shoulder (Fig. 9*a* and *b*).

Figure 11 shows the relationship between the failure load during overlap shear testing and the bonded area in completed welds. The failure load increased when the

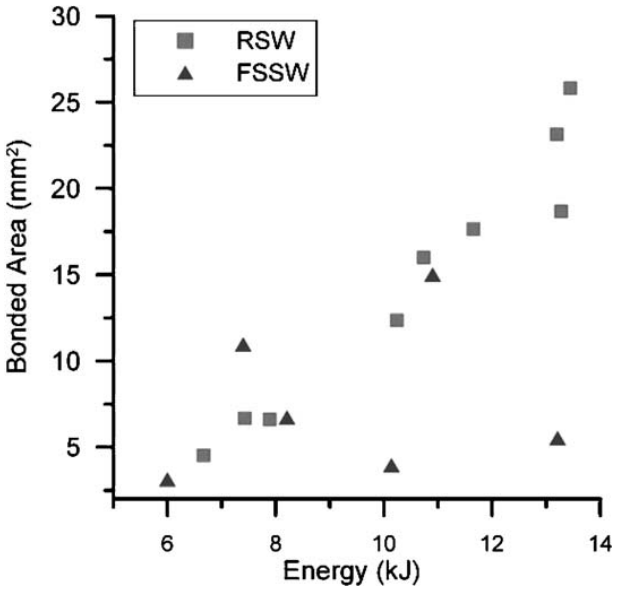

10 Bonded area versus energy

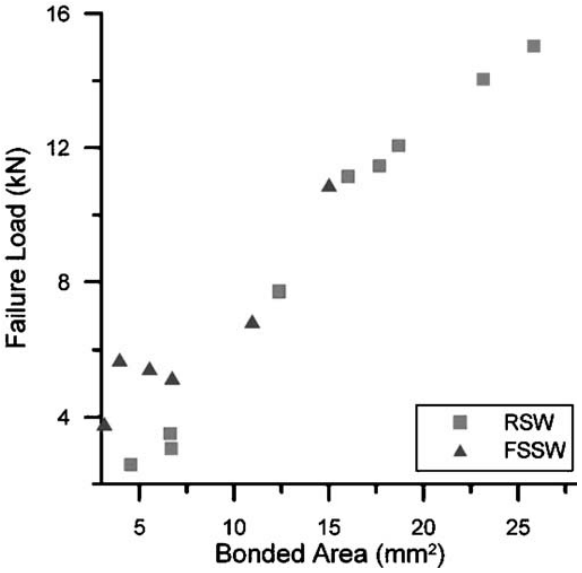

11 Failure load versus bonded area

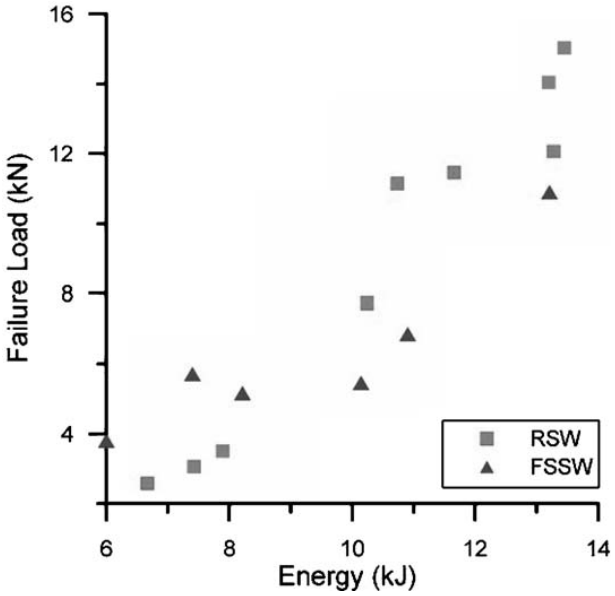

12 Failure load versus total energy

bonded area increased for both processes. Similar test output has been found during FSSW of both Al alloy and Mg alloy sheet materials.[14] This indicates similar material properties in terms of tensile strength and hardness within the stir zone and FZ for FSSW and RSW welds respectively.

Figure 12 shows the relationship between energy input during FSSW and the failure load during overlap shear testing. Higher failure loads were produced when the energy input during spot welding increased. In this connection, it is worth noting the parallel relationship of energy input and failure load between the two welding processes. Differences in bonded area of fracture surfaces of high and low energy welds are shown in Fig. 7*c–e*. Friction stir spot welding welds produced both pull-out and interfacial fracture for high and low energy input welds.

The bonded area seems to provide a reasonable basis for comparing the RSW and FSSW outputs (Fig. 11). A similar trend is observed between RSW and FSSW welds. Peak failure loads of 15 and 11 kN were obtained for RSW and FSSW welds respectively. Owing to the geometry of the unbonded regions failure loads are greater for RSW welds. Energy requirements also show a comparable trend (Fig. 12). Resistance spot welding welds show a relatively linear relationship with energy and failure loads. With lower energy input FSSW welds show a non-linear relationship. This is likely due to the change from only pin penetration to a combination of pin and shoulder penetration. Higher failure load energy inputs are relatively similar to RSW energy inputs.

Additional factors

Aesthetically, the surface finish of welds produced using RSW are superior to those produced using FSSW. In some automotive application the smooth surface finish produced by RSW is desired, and the FSSW keyhole would be considered unacceptable. Recent advancements in tool design have produced a retractable pin tool (RPT) which refills the remaining keyhole without affecting the mechanical properties of the spot weld.[19] This, however, increases the cost and complexity of FSSW equipment. Discoloration of spot welds in steel is not considered a problem, because the surface is typically finished by painting. If required, oxidation of the surface in FSSW can be prevented by adequate shielding using inert gas, but this too increases the cost of the process.

Prevention of galvanic corrosion for this particular sheet of DP600 is facilitated with a hot dip galvanised zinc coating. Studies have shown during RSW of Zn coated steel annular zinc braze forms at the faying surface around the FZ.[17] Furthermore during the first two cycles of welding the molten Zn coating is pushed away from the FZ.[20] The mechanical nature of FSSW limits interference of Zn coatings during FSSW. Previous studies show the peak temperatures reaching $0{\cdot}9T_m$ of the BM,[12,13] which in the case for DP600 is well above the melting temperature of Zinc. Figure 7*c* and *d* shows evidence of an annular braze forming around the RSW and FSSW weld.

The effect of the zinc coating on the RSW process is known to significantly reduce electrode contact tip life. Studies have shown that electrode degradation may be delayed through the use of conductive coatings that prevent alloying between the copper electrode and zinc coating.[21] The net result of the zinc coating is an increase in consumable cost. The FSSW process does not appear to be affected by this as there are no studies to show an observable effect of the zinc coating on tool wear.

Results from the energy calculations show that energy consumption is similar for both processes. Faster cycle times in RSW result in a greater productivity than FSSW. Owing to the widespread implementation of RSW, the infrastructure and support system is already in place. The FSSW process is not yet used extensively in the automotive industry, and as a result the infrastructure and support is not yet in place. Furthermore, the FSSW process requires additional fixtures owing to its mechanical nature. At the moment RSW is a more cost effective process; however, further advancements in FSSW will make it more economically competitive.

It must be stressed at the outset that the objective in this particular study involves comparing the factors which determine the overlap shear strength properties of

RSW and FSSW spot welded joints in dual phase steel. A single pulse welding schedule was used in the RSW case, and optimising the welding schedule to minimise centreline growth of the columnar grains may further improve mechanical properties. Also a smooth pin FSSW tool design was used when welding dual phase sheet a limited range of welding parameter settings. As a result, the output produced in this paper should be regarded only as a nominal starting point for future research. The fracture loads produced during overlap shear testing of spot welded dual phase sheet should therefore are not indicative of the highest values which can be obtained when the steel sheet is spot welded.

Conclusions

In this study, mechanical and metallurgical properties of RSW and FSSW DP600 welds were compared. A correlation was found among failure loads, energy requirements and bonded area for both processes. Also, partial tensile shear can be used to understand the initiation and propagation of cracks. From this it can be concluded that:

1. The microstructure of the HAZ is similar in both RSW and FSSW welds in DP600 AHSS. The IC and FG subregions consist of a mixture of martensite and ferrite. The martensite occurs as islands in a ferrite matrix, with increasing martensite volume fraction towards the weld centreline.

2. The FSSW weld microstructure consisted of a TMAZ between the HAZ and the stir zone. This region consists of a mixture of lathy martensite, bainite and ferrite. Martensite is observed in both the FZ and stir zone of the RSW and FSSW welds respectively. The morphology of the microstructure, however, is very different for both processes.

3. The microstructure hardness is similar in the FZ and stir zone for RSW and FSSW respectively. The hardness decreases from the weld centreline into the BM; however, the HAZ in RSW case was narrower.

4. In the case of RSW, fracture initiates between the two sheets and propagates through the interface of the material. For the FSSW welds, fracture initiates at the unbonded region and propagates through the upper sheet just under the shoulder, suggesting a need for further optimisation of tool geometry.

5. The failure load increased when the bonded area increased for both processes. Failure loads also increased with increasing energy input into the weld.

6. The weld efficiency of both processes is similar for DP600 sheet steel when compared on a basis of fracture load versus energy or bonded area.

Acknowledgement

The authors would like to acknowledge the funding and support from Auto21 (www.auto21.ca), one of the Networks of Centres for Excellence supported by the Canadian Government.

References

1. K. Kunishige, N. Yamauchi, T. Taka and N. Nagao: Proc. SAE Int. Cong. Expos., Detroit, MI, USA, 1983, February–March, SAE, Paper 830632.
2. P. K. Ghosh P. C. Gupta, O. M. Pal, R. Avtar, B. K. Jha and V. Sagar Dwivedi: *ISIJ Int.*, 1993, **33**, 807–815.
3. P. K. Ghosh P. C. Gupta, R. Avtar and B. K. Jha: *Weld. J.*, 1991, **70**, 7-s–14-s.
4. Z. Feng, M. L. Santella and S. A. David: Proc. SAE World Cong. Exhib., Detroit, MI, USA, April 2005, Paper no. 2005-01-1248.
5. W. J. Kyffin, J. Martin, A. C. Addison and P. L. Threadgill: Proc. 12th Conf. on 'Sheet metal welding', Livonia, MI, USA, May 2006, TWI, Paper 2–2.
6. A/SP: 'AHSS applications recommendations', 2005 American Iron and Steel Institute.
7. G. Tawade and G. Boudreau: Proc. 2004 Steel Seminar, Detroit, February 2004, American Iron and Steel Institute, Paper 2–7.
8. O. T. Midling, E. J. Morley and A. Sandvik: European patent specification 0 752 926 B1, 1995.
9. P. Su, A. Gerlich, T. H. North and G. J. Bendzsak: *Sci. Technol. Weld. Join.*, 2006, **11**, 163–169.
10. A. Gerlich, P. Su and T. H. North: 'Generation and stir zone dimensions in friction stir spot welds', Document no. 2006-01-0971, SAE, 2006, **37**, 2773–2786.
11. G. A. C. A. Gerlich and T. H. North*: Metall. Trans. A*, 2006, **37**, 2773–2786.
12. P. Su, A. Gerlich, T. H. North and G. J. Bendzsak: 'Materials forum', Vol. 29, 290–294.
13. P. Su, A. Gerlich and T. H. North: *Sci. Technol. Weld. Join.*, 2006, **29**, 647–652.
14. ANSI/AWS/SAE/D8·9–97: 'Recommended practices for test methods for evaluating the resistance spot welding behavior of automotive steels', 1997.
15. C. D. Johnson (ed.): 'Handbook of electrical and electronic technology', 1st edn, 51–57; 1996, Englewood Cliffs, NJ, Prentice Hall.
16. P. Su, A. Gerlich and T. H. North: *J. Mater. Sci.*, 2005, **40**, 6473–6481.
17. S. A. G. T. W. Eagar: *Metall. Trans. B*, 1986, **17B**, 887–901.
18. F. S. Lepera: *J. Met.*, 1980, 38–39.
19. R. J. Ding: Proc. Int. Conf. on 'Trends in welding research', Pine Mountain, GA, USA, June 1998, ASM, 585–589.
20. W. Tan, Y. Zhou and H. W. Kerr: *Metall. Mater. Trans. A*, 2002, **33A**, 2667–2676.
21. N. Z. S. Dong, C. Cheng, Y. Shi and B. Chang: Trans. *Nonfer. Met. Soc. Chin.*, 2005, **15**, 1219–1225.